JACS
JOURNAL OF THE AMERICAN CHEMICAL SOCIETY

Article

pubs.acs.org/JACS

Metal–Organic-Frameworks-Derived General Formation of Hollow Structures with High Complexity

Lei Zhang,[†] Hao Bin Wu,[†] and Xiong Wen (David) Lou*

School of Chemical and Biomedical Engineering, Nanyang Technological University, 62 Nanyang Drive, 637459 Singapore

Supporting Information

ABSTRACT: Increasing the complexity of hollow structures, in terms of chemical composition and shell architecture, is highly desirable for both fundamental studies and realization of various functionalities. Starting with metal–organic frameworks (MOFs), we demonstrate a general approach toward the large-scale and facile synthesis of complex hollow microboxes via manipulation of the template-engaged reactions between the Prussian blue (PB) template and different alkaline substances. The reaction between PB microcubes with NaOH solution leads to the formation of $Fe(OH)_3$ microboxes with controllable multishelled structure. In addition, PB microcubes will react with the conjugate bases of metal oxide based weak acids, generating multicompositional microboxes (Fe_2O_3/SnO_2, Fe_2O_3/SiO_2, Fe_2O_3/GeO_2, Fe_2O_3/Al_2O_3, and Fe_2O_3/B_2O_3), which consist of uniformly dispersed oxides/hydroxides of iron and another designed element. Such complex hollow structures and atomically integrated multiple compositions might bring the usual physiochemical properties. As an example, we demonstrate that these complex hollow microboxes, especially the Fe_2O_3/SnO_2 composite microboxes, exhibit remarkable electrochemical performance as anode materials for lithium ion batteries.

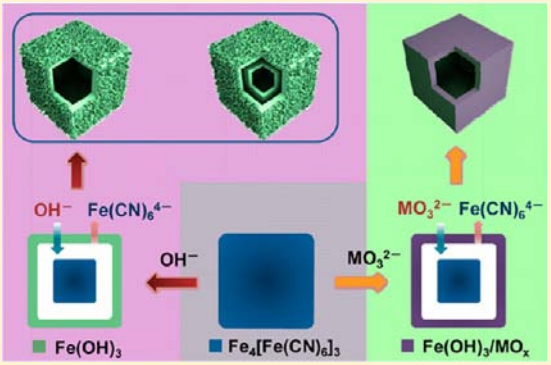

INTRODUCTION

Hollow microsized/nanosized particles are of great significance because of their unique structure-dependent properties and promising applications in many areas.[1−9] Typical syntheses of hollow particles involve the growth of desirable shells with the assistance of removable or sacrificial template particles. To realize desirable functionalities and maximize the structural advantages, hollow particles with high complexity, such as multiple layers of shells or multiple compositions, are highly desirable. However, most of the available hollow particles prepared via multistep templating processes exhibit relatively simple configurations, such as single-shelled spheres of one composition.

Templating methods have been considered as the most representative and straightforward approach toward hollow structures, which involve the controlled assembling of the designed materials on various removable templates, such as monodisperse silica/polymer latex spheres and emulsion micelles.[1,6,10] Although conceptually versatile, the templating strategy practically has quite a few difficulties, ranging from the tedious procedure to the incompatibility issue between the desired materials and the template surfaces. Meanwhile, several novel approaches toward hollow structures have been developed on the basis of different principles, including the Kirkendall effect,[4,5] galvanic replacement,[2,11] chemical etching,[12,13] ionic exchange,[3,14,15] self-assembly,[16] thermal decomposition, etc.[17,18] For example, template-engaged methods (i.e., galvanic replacement, chemical etching) create hollow cavities in preformed solid template particles via manipulation of the different physicochemical or chemical properties between the sacrificial templates and the shell materials.[2,11−13] Such template-engaged approaches are very effective to form hollow particles with various shapes, yet their versatility would be largely determined by the variety of the available sacrificial templates and the precursors of shell materials.[19]

Notwithstanding the above-mentioned advances in synthetic methods, hollow particles reported so far with high quality usually possess simple configurations. Increasing the complexity of hollow structures, in terms of chemical composition and shell architecture, is highly desirable for both fundamental studies and realization of various functionalities. This objective could possibly be achieved via complicated procedures, such as repeated templating methods.[13,14,20,21] Nevertheless, it is extremely challenging to highly integrate multiple compositions into the hollow particles based on the protocols established so far, since different materials with distinct physical/chemical properties could hardly be incorporated simultaneously into the synthesis process.

Herein, we demonstrate a general approach toward the large-scale and facile synthesis of complex hollow cubic microsized particles (in short, hollow microboxes) via precise manipulation of the template-engaged reactions between a unique metal–organic frameworks (MOFs) template and different substances.

Received: February 17, 2013
Published: June 27, 2013

   dx.doi.org/10.1021/ja401727n | J. Am. Chem. Soc. 2013, 135, 10664−10672

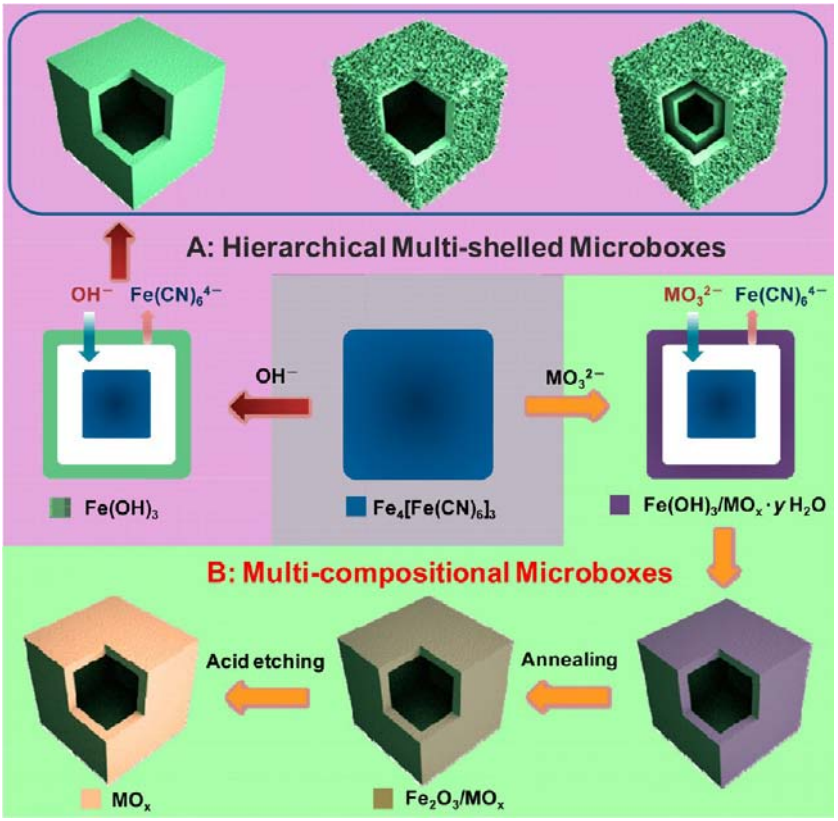

Figure 1. Schematic illustration of the formation of hierarchical multishelled (route A) and multicompositional (route B) metal oxides microboxes starting with metal−organic frameworks templates. Metal oxides microboxes were synthesized by manipulating the ion exchange reaction between a proper alkaline precursor (strong base or conjugate base of the weak acid) and a sacrificial PB by the following reactions. Route A: 12 $OH^-_{(aq)}$ + $Fe_4[Fe(CN)_6]_{3\ (s)} \rightarrow 3\ Fe(CN)_6^{4-}{}_{(aq)} + 4\ Fe(OH)_{3(s)}$. Route B (for the case Sn): $6SnO_3^{2-}{}_{(aq)} + Fe_4[Fe(CN)_6]_{3(s)} + 6(1 + x)H_2O \rightarrow 3Fe(CN)_6^{4-}{}_{(aq)} + 4\ Fe(OH)_{3(s)} + 6\ SnO_2{\cdot}xH_2O_{(s)}$.

By controlling the reaction/diffusion kinetics, we have synthesized iron oxide/hydroxide hollow microboxes with hierarchical multishelled structures. Furthermore, the oxides/hydroxides of several metals/metalloids (Sn, Si, Ge, Al, B, etc.) can be incorporated into the iron oxide/hydroxide microboxes by coupling the condensation reactions. Our results show the feasibility and versatility of template-engaged syntheses of complex hollow particles and would shed some light on the fabrication of other complex hollow structures.

EXPERIMENTAL SECTION

Chemicals. Polyvineypirrolydone (K30), $K_4Fe(CN)_6{\cdot}3H_2O$, HCl, NaOH, $K_2SnO_3{\cdot}3H_2O$, $NaAlO_2$, $NaBO_2{\cdot}4H_2O$ were purchased from Sigma Aldrich. Na_2SiO_3 was purchased from Kanto Chemical Co., Inc. The Na_2GeO_3 powders were prepared by a solid state reaction route in which a stoichiometric mixture of Na_2CO_3 and GeO_2 was heated at 900 °C for 10 h.[22]

Synthesis of Prussian Blue Microcubes. Prussian blue microcubes were prepared according to our previous report.[23] In a typical procedure, polyvineypirrolydone (PVP, K30, MW ≈ 40 000, 3.8 g) and $K_4Fe(CN)_6{\cdot}3H_2O$ (0.11 g) were added to a HCl solution (0.1 M, 50 mL) under magnetic stirring. After the mixture was stirred for 30 min, a clear solution was obtained. The bottle was then placed into an electric oven and heated at 80 °C for 24 h. The obtained blue product was filtered and washed several times with deionsized water and absolute ethanol and finally dispersed into 20 mL of ethanol for further use.

Synthesis of $Fe(OH)_3$ Microboxes at Room Temperature. The $Fe(OH)_3$ microboxes were obtained by the reaction of $Fe_4[Fe(CN)_6]_3$ microcubes with NaOH at room temperature. Typically, 10 mL of above $Fe_4[Fe(CN)_6]_3$ cubes suspension in ethanol was mixed with 17 mL of 0.02 M NaOH aqueous solution. After the mixture was shaken by hand for about 5 min, the as-prepared product was collected by several rinse−centrifugation cycles. For synthesis of yolk-shelled $Fe(OH)_3$ microboxes, a NaOH solution with a different concentration (0.2 M) was used. Hollow Fe_2O_3 microboxes were made by annealing the corresponding hollow $Fe(OH)_3$ microboxes precursor at 300 °C in air for 6 h with a slow heating rate of 0.5 °C min^{-1}.

Synthesis of Multishelled $Fe(OH)_3$ Microboxes under Hydrothermal Conditions. The hierarchically multishelled $Fe(OH)_3$ microboxes were obtained by the reaction of $Fe_4[Fe(CN)_6]_3$ cubes with NaOH under hydrothermal conditions. Typically, 5 mL of $Fe_4[Fe(CN)_6]_3$ cubes dispersed in ethanol was added to 20 mL of 0.2 M NaOH aqueous solution. The suspension was transferred to a 60 mL Teflon-lined stainless steel autoclave, which was then heated in an air flow electric oven at 80 °C for 10 h. After the autoclave cooled naturally, the as-prepared products were collected by several rinse−centrifugation cycles. For synthesis of multishelled $Fe(OH)_3$ microboxes, NaOH solutions with different concentrations (2.0, 3.0, and 4.0 M) were used. Hollow Fe_2O_3 microboxes were made by annealing the corresponding hollow $Fe(OH)_3$ microboxes precursor at 300 °C in air for 6 h with a slow heating rate of 0.5 °C min^{-1}.

Synthesis of Fe_2O_3/SnO_2 Microboxes at Room Temperature. The $Fe(OH)_3/SnO_2{\cdot}xH_2O$ microboxes were obtained by the reaction of $Fe_4[Fe(CN)_6]_3$ microcubes with $K_2SnO_3{\cdot}3H_2O$ at room temperature. Typically, 10 mL of the above $Fe_4[Fe(CN)_6]_3$ cubes suspension in ethanol was mixed with 17 mL of deionized water. To this suspension, 0.12 g of potassium stannate trihydrate was added. After the mixture was shaken by hand for about 2 min, the as-prepared product was collected by several rinse−centrifugation cycles. Fe_2O_3/SnO_2 microboxes were obtained by annealing the as-prepared $Fe(OH)_3/SnO_2{\cdot}xH_2O$ microboxes precursor at 500 °C in air for 6 h

dx.doi.org/10.1021/ja401727n | J. Am. Chem. Soc. 2013, 135, 10664−10672

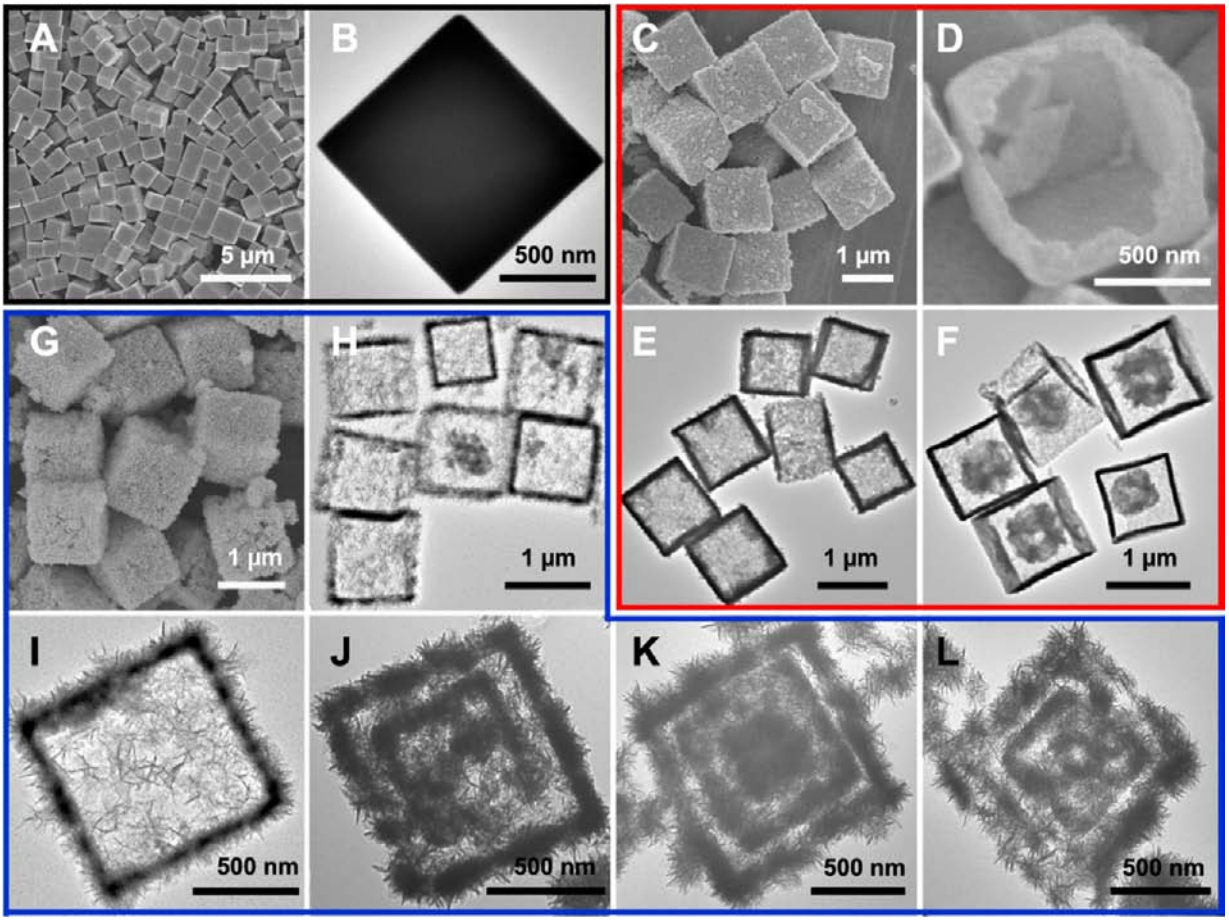

Figure 2. Formation of hierarchical $Fe(OH)_3$ microboxes by PB templating at room temperature and hydrothermal conditions: FESEM (A) and TEM (B) images of $Fe_4[Fe(CN)_6]_3$ microcubes; FESEM (C, D) and TEM (E, F) images of $Fe(OH)_3$ microboxes (C–E) and yolk-shelled $Fe(OH)_3$ microboxes (F) synthesized at room temperature; FESEM (G) and TEM (H-L) images of hierarchically single-shelled (G–I) and multiple-shelled (J–L) $Fe(OH)_3$ microboxes synthesized under hydrothermal conditions.

with a slow heating rate of 0.5 °C min^{-1}. To obtain SnO_2 microboxes, Fe_2O_3/SnO_2 microboxes were treated with a 2.0 M HCl aqueous solution at ambient temperature.

Synthesis of Fe_2O_3/SiO_2, Fe_2O_3/GeO_2, Fe_2O_3/Al_2O_3, and Fe_2O_3/B_2O_3 Microboxes at Room Temperature. Compared with the synthesis of Fe_2O_3/SnO_2 microboxes, 0.12 g of potassium stannate trihydrate was replaced by 0.12 g of Na_2SiO_3, Na_2GeO_3, $NaAlO_2$, or $NaBO_2{\cdot}4H_2O$, respectively. The following procedure is the same as that for the synthesis of Fe_2O_3/SnO_2 microboxes.

Characterization. X-ray diffraction (XRD) patterns were collected on a Bruker D8 Advanced X-ray diffractometer with Ni filtered Cu Kα radiation (λ = 1.5406 Å) at a voltage of 40 kV and a current of 40 mA. Field-emission scanning electron microscope (FESEM) images were acquired on a JEOL JSM-6700F microscope operated at 5 kV. Transmission electron microscopy (TEM) images were taken on JEOL JEM-2010 and JEOL JEM-2100F microscopes. Energy-dispersive X-ray (EDX) analysis and elemental mapping were performed using the energy-dispersive X-ray spectroscopy attached to the JSM-6700F and JEM-2100F, respectively. Nitrogen sorption measurements were performed on an Autosorb 6B apparatus at liquid N_2 temperature. The chemical compositions of multicompositional microboxes were measured using inductively coupled plasma (ICP) optical emission spectroscopy with a Perkin-Elmer ICP Optima 2000DV.

Electrochemical Measurements. The electrochemical tests were carried out in two-electrode Swagelok cells. The working electrodes consist of 70% of active material, 20% of conductive carbon black (Super-P-Li), and 10% of polymer binder (polyvinylidene fluoride, PVDF). The electrolyte is 1.0 M $LiPF_6$ in a mixture of ethylene carbonate and diethyl carbonate (1/1 by weight). A lithium disk was used as both the counter and reference electrode. Cell assembly was carried out in an Ar-filled glovebox with moisture and oxygen concentrations below 1.0 ppm. The charge–discharge tests were performed on a NEWARE battery tester.

■ RESULTS AND DISCUSSION

Our strategy for synthesizing complex hollow microboxes is based on the template-engaged reactions between a unique MOFs template and different substances. The complexity of the resultant hollow microboxes can be achieved in two aspects, namely, the hierarchical multishelled structure and multi-compositions with atomically integrated oxides/hydroxides of iron and several metal/metalloids, as depicted in Figure 1. Microsized Prussian blue (PB, $Fe_4[Fe(CN)_6]_3$) crystals with a cubic shape (denoted as PB microcubes) are employed as the template. Route A illustrates the formation of hollow microboxes with different structural complexity, from single shell to multishell with hierarchical architectures. Route B describes the synthesis of multicompositional hollow microboxes consisting of uniformly dispersed oxides/hydroxides of iron and another designed element. These complex hollow structures are prepared by precisely controlling the chemical reactions between the PB microcubes template and a proper alkaline precursor (a strong base or a conjugate base of a metal/

dx.doi.org/10.1021/ja401727n | J. Am. Chem. Soc. 2013, 135, 10664–10672

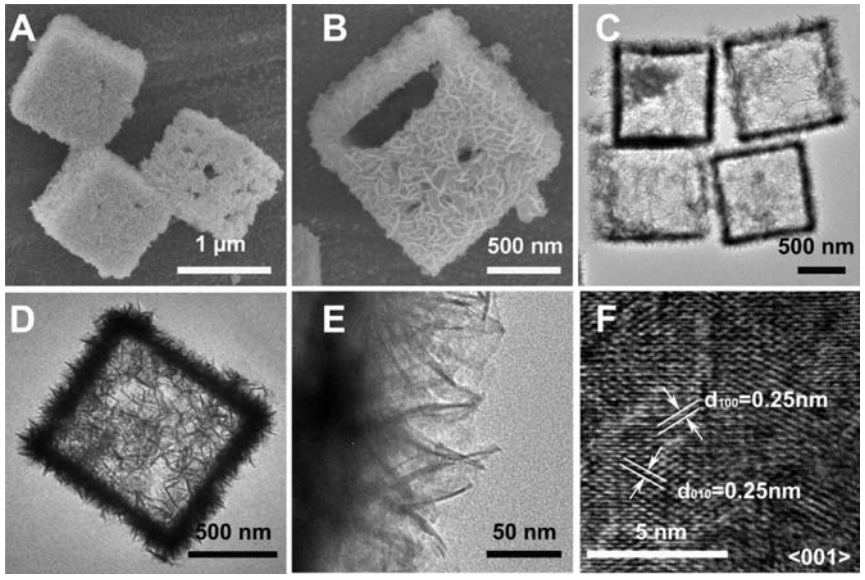

Figure 3. FESEM (A, B) and TEM (C–F) images of hierarchically single-shelled Fe_2O_3 microboxes obtained by the reaction of $Fe_4[Fe(CN)_6]_3$ cubes with 0.2 M NaOH under hydrothermal conditions.

metalloid oxide based weak acid), which will be discussed in detail shortly.

Prussian blue is considered as the first synthetic coordination compound (or more commonly called MOFs), which is a mixed-valence iron(III) hexacyanoferrate(II) compound with a face-centered-cubic (*FCC*) structure (JCPDS card no. 73-0687; space group *Fm3m*, $a = b = c = 10.13$ Å, $\alpha = \beta = \gamma = 90°$).[24] PB microcubes of about 1 μm with high morphological uniformity and phase purity (Figure 2A,B, Figure S1 and Figure S2 in the Supporting Information) were synthesized and applied as the template in view of the unusual chemical properties and the scarcity of fabricating nanostructured materials using MOFs based templates.[23] PB is insoluble in water with a very small solubility product constant ($K_{sp} = 3.3 \times 10^{-41}$). However, in alkaline solution, PB undergoes an ion exchange reaction as described below:

$$12OH^-_{(aq)} + Fe_4[Fe(CN)_6]_{3(s)} \rightarrow 3Fe(CN)_6^{4-}{}_{(aq)} + 4Fe(OH)_{3(s)} \quad (1)$$

The Fe(III) ions in PB associate with hydroxide ions to form insoluble $Fe(OH)_3$ ($K_{sp} = 2.6 \times 10^{-39}$), which is driven by the high concentration of hydroxide ions in an alkaline solution. To investigate the transformation of PB in an alkaline solution, we first carry out the reaction using PB microcubes and NaOH solution (Figure 1, route A). The products were examined by FESEM and TEM. After reacting with a dilute NaOH solution (0.02M) at room temperature, the PB microcubes were converted into microboxes with large interior cavity (Figure 2C–E). Remarkably, microboxes with higher structural complexity could be simply obtained via a similar process with increased reaction and diffusion kinetics. For instance, when NaOH solution with a higher concentration (0.2 M) was used, yolk-shelled microboxes with well-defined porous cores were obtained as the final product (Figure 2F, Figure S3 and Figure S4 in Supporting Information). The reaction could be further promoted by increasing the concentration of alkaline solution and/or reaction temperature, which results in even more complex structures. After reaction at an elevated temperature of 80 °C with a 0.2 M NaOH solution, the product was mostly composed of single-shelled microboxes, of which the shell was constructed by sheetlike subunits (Figure 2G–I and Figure S5 in Supporting Information). When concentrated NaOH solution of 2.0–4.0 M was used for the synthesis, microboxes with multiple shells and similar hierarchical architectures were formed (Figure 2J–L and Figure S6 in Supporting Information). It is postulated that the inward diffusion of OH^- and precipitation of $Fe(OH)_3$ are promoted with higher temperature and alkaline concentration. Hence, after the initial formation of the outer shell, an intershell of $Fe(OH)_3$ would be precipitated before the Fe species migrate outward and join the outer shell. Eventually the multishell structures are obtained.

The chemical process that leads to the formation of hollow structures can be rationalized as follows: the ion exchange reaction first takes place at the interface between the solid PB microcubes and liquid alkaline solution, leading to the formation of a thin layer of $Fe(OH)_3$ on the PB surface. As the reaction proceeds, OH^- ions continue to flow inward to supply the ion exchange reaction, while the precipitation of $Fe(OH)_3$ clusters on the preformed $Fe(OH)_3$ layer and the outward diffusion of $Fe(CN)_6^{4-}$ ions are anticipated (Figure S7 in Supporting Information). If the reaction proceeds slowly, the whole PB microcubes are gradually consumed accompanied by the growth of the $Fe(OH)_3$ shell, which eventually evolve into well-defined $Fe(OH)_3$ microboxes with large interior cavity. Meanwhile, the inward diffusion of OH^- ions and the ion exchange reaction can be significantly accelerated in concentrated alkaline solution at an elevated temperature. In such circumstance, a secondary layer of $Fe(OH)_3$ would precipitate on the inner core prior to its complete consumption, resulting in the formation of yolk-shelled or multishelled structures.

The as-prepared $Fe(OH)_3$ microboxes exhibit an amorphous texture as determined by powder X-ray diffraction (XRD) analysis, which could be easily converted to α-Fe_2O_3 via a low-temperature annealing process (Figure S8 in Supporting Information). The morphology, hollow structure, and sheetlike subunits are all well preserved, indicating the good structural stability of the $Fe(OH)_3$ and as-derived Fe_2O_3 microboxes

dx.doi.org/10.1021/ja401727n | J. Am. Chem. Soc. 2013, 135, 10664–10672

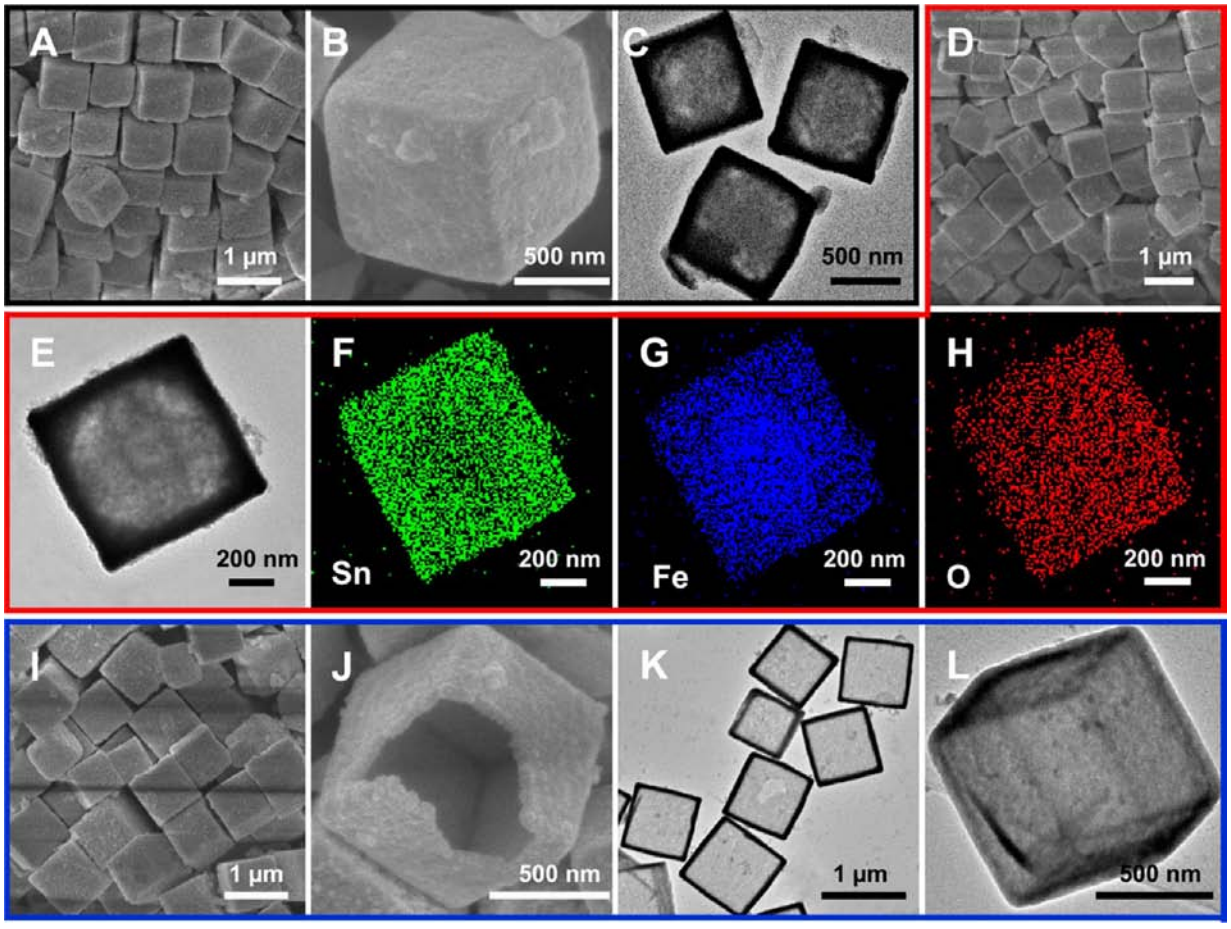

Figure 4. Formation of multicompositional Fe_2O_3/SnO_2 microboxes by PB templating at room temperature: FESEM (A, B) and TEM (C) images of $Fe(OH)_3/SnO_2{\cdot}xH_2O$ microboxes; FESEM (D), TEM (E) images, and EDX-elemental mapping images (F–H) of one Fe_2O_3/SnO_2 microbox shown in (E); FESEM (I, J) and TEM (K, L) images of SnO_2 microboxes.

(Figure 3). The high-resolution TEM (HRTEM) image in Figure 3F shows a crystalline character with a lattice spacing of 0.25 nm, which is close to the interplanar distance of the (010) and (100) planes of Fe_2O_3. Such interesting structures render the $Fe(OH)_3$ and Fe_2O_3 microboxes with relatively high Brunauer–Emmett–Teller (BET) surface areas of 175–255 $m^2\ g^{-1}$ and 92–174, respectively (Figures S9–S11 in Supporting Information).

The ion exchange reaction between PB and strong base (e.g., NaOH and KOH) only results in products with single composition, namely, $Fe(OH)_3$ or Fe_2O_3. We further replace the strong base with the conjugate base of a metal/metalloid oxide based weak acid, which is a weak base in nature due to the partial hydrolysis. Under optimized conditions, the hydrolysis of the conjugate base and the ion exchange of PB might take place simultaneously (Figure 1, route B). To demonstrate the feasibility of such an approach, we select K_2SnO_3 as an example, which can partially hydrolyze to form tin hydroxide (or oxide hydrate) and generate an alkaline environment:

$$SnO_3^{2-}{}_{(aq)} + (1 + x)H_2O \rightarrow SnO_2{\cdot}xH_2O_{(s)} + 2OH^-{}_{(aq)} \quad (2)$$

If this hydrolysis reaction (eq 2) could be coupled with the ion exchange reaction of PB (eq 1), the overall process would result in the simultaneous and stoichiometric condensation of iron and tin hydroxide/oxide based on the following reaction:

$$6SnO_3^{2-}{}_{(aq)} + Fe_4[Fe(CN)_6]_{3(s)} + 6(1 + x)H_2O \rightarrow 3Fe(CN)_6^{4-}{}_{(aq)} + 4Fe(OH)_{3(s)} + 6SnO_2{\cdot}xH_2O_{(s)} \quad (3)$$

To verify our hypothesis, the product of the reaction between PB microcubes and K_2SnO_3 solution was characterized thoroughly. As shown in Figure 4A–C, the product also consists of hollow microboxes with smooth surface, however, the shell of which is slightly thicker and displays a denser texture compared with that of $Fe(OH)_3$ microboxes. Certain porosity is still expected in the shell, as suggested by the moderate BET surface area of 44 $m^2\ g^{-1}$ even without any hierarchical or multishelled structure (Figure S12 in Supporting Information). Energy-dispersive X-ray spectroscopy (EDX, Figure S13 in Supporting Information) analysis of the as-prepared microboxes evidently reveals the presence of Sn, resulting from the hydrolysis of K_2SnO_3 as expected. The Fe/Sn atomic ratio determined by the ICP analysis is about 2/3, which is in good agreement with the stoichiometry of $Fe(OH)_3$ and $SnO_2{\cdot}xH_2O$ in eq 3. This further suggests the successful coupling of the ion exchange reaction (eq 1) and the hydrolysis reaction (eq 2). The amorphous composite microboxes (denoted as $Fe(OH)_3/SnO_2{\cdot}xH_2O$ microboxes) were annealed at 500 °C in air to convert to the oxide form (denoted as Fe_2O_3/SnO_2 microboxes, Figure 4D and Figure S14 in Supporting Information). The XRD pattern of the annealed

dx.doi.org/10.1021/ja401727n | J. Am. Chem. Soc. 2013, 135, 10664–10672

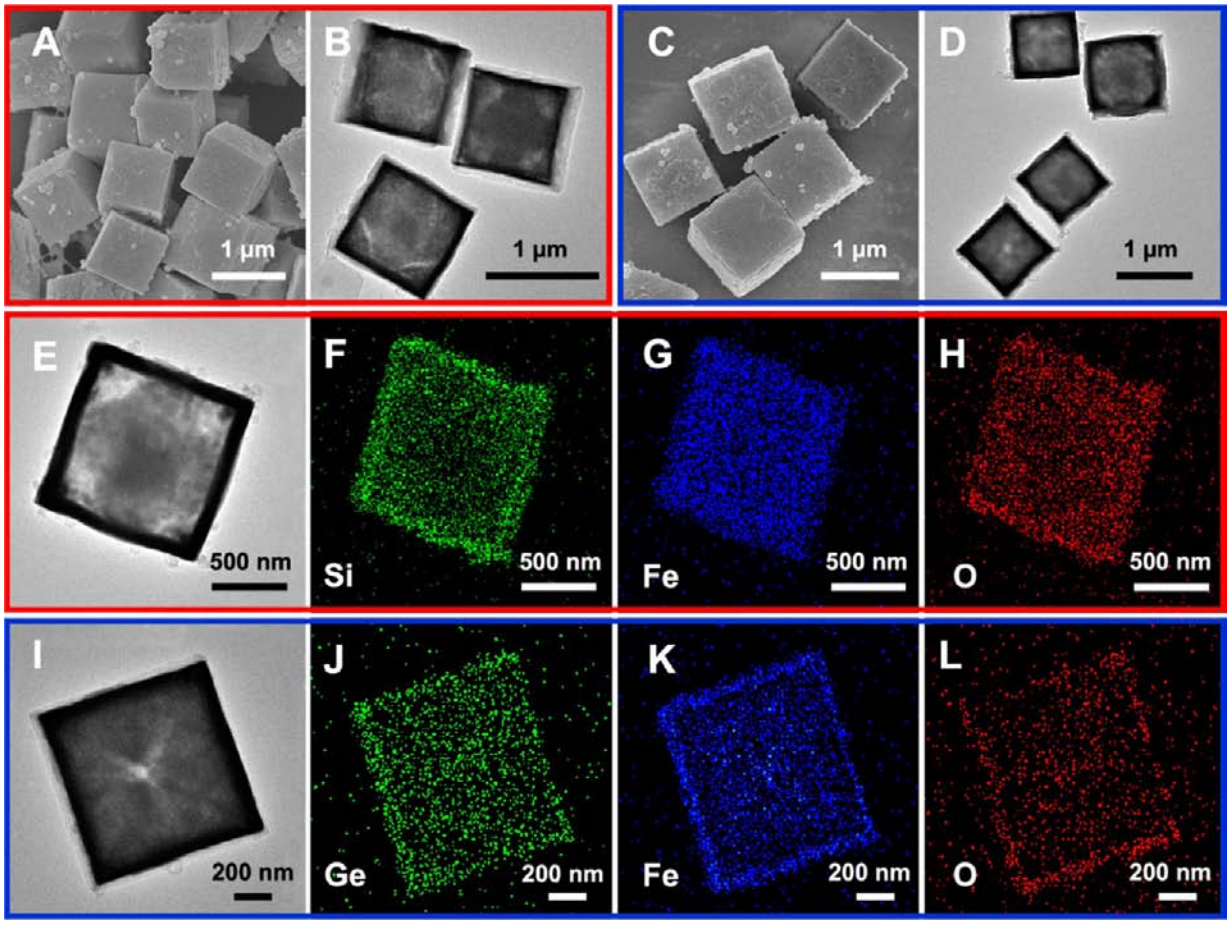

Figure 5. Formation of multicompositional Fe_2O_3/SiO_2 and Fe_2O_3/GeO_2 microboxes at room temperature: FESEM (A), TEM (B, E) images, and EDX-elemental mapping images (F−H) of one Fe_2O_3/SiO_2 microbox shown in (E); FESEM (C), TEM (D, I) images and EDX-elemental mapping images (J−L) of one Fe_2O_3/GeO_2 microbox shown in (I).

sample (Figure S15 in Supporting Information) can be assigned to a mixture of α-Fe_2O_3 (JCPDS no. 33-0664) and rutile SnO_2 (JCPDS no. 41-1445), which is similar to that of previously reported mixture of α-Fe_2O_3 and SnO_2.[25] The broad diffraction peaks also reveal the low crystallinity of Fe_2O_3/SnO_2 microboxes, possibly due to mutual inhibition of crystal growth of the highly dispersed Fe_2O_3 and SnO_2. To illustrate the spatial distribution of Fe_2O_3 and SnO_2 in the composite microboxes, elemental mapping is performed on a representative Fe_2O_3/SnO_2 microbox (Figure 4E) under TEM observation. The elemental mapping results (Figure 4F−H) demonstrate the generally uniform distribution of Sn and Fe within the microbox, which corresponds to the SnO_2 and Fe_2O_3 crystallites. After selectively dissolving Fe_2O_3 with a 2.0 M HCl aqueous solution, single-compositional SnO_2 microboxes were obtained as confirmed by electron microscope images (Figure 4I−L and Figure S16 in Supporting Information) and XRD analysis (Figure S15 in Supporting Information). The SnO_2 microboxes remain intact, whereas the removal of Fe_2O_3 makes the shell more porous as evidenced by the improved transparency of the microboxes and some visible pores in TEM images (Figure 4K,L and Figure S16B in Supporting Information) and the significant increase of BET surface area from 43 $m^2\ g^{-1}$ for Fe_2O_3/SnO_2 microboxes (Figure S17 in Supporting Information) to 89 $m^2\ g^{-1}$ for SnO_2 microboxes (Figure S18 in Supporting Information).

The above analysis unambiguously indicates the high integration and uniform dispersion of iron and tin hydroxides/oxides in the composite microboxes. This compositional uniformity is derived from the simultaneous formation of Fe- and Sn-based species during the unique template-engaged process (Figure 1, route B). The alkaline environment provided by the hydrolysis of K_2SnO_3 triggers the conversion from PB microcubes to $Fe(OH)_3$ microboxes similar to that in route A. Meanwhile, the consumption of hydroxide ions promotes the in situ and stoichiometric precipitation of amorphous $SnO_2{\cdot}xH_2O$ during the formation of $Fe(OH)_3$ shell. Therefore, driven by such unique coupled ion exchange/hydrolysis reactions, two different compositions can be hybridized in atomic scale within the shell of hollow particles.

Remarkably, this approach to synthesize iron-based multicompositional microboxes can be extended to incorporate several other metal/metalloid oxides when the proper alkaline precursor is used. For example, we have successfully prepared Fe_2O_3/SiO_2 and Fe_2O_3/GeO_2 microboxes as demonstrated in Figure 5, using Na_2SiO_3 and Na_2GeO_3 as the alkaline precursors, respectively. EDX analysis of the as-prepared Fe_2O_3/SiO_2 and Fe_2O_3/GeO_2 microboxes confirms the coexistence of Fe/Si and Fe/Ge elements in the composite microboxes with estimated atomic ratios of about 1/1 and 4/3, respectively (Figures S19 and S20 in Supporting Information). Other elements from the nearby IIIA group, such as Al and B, can also be easily hybridized into the multicompositional

dx.doi.org/10.1021/ja401727n | J. Am. Chem. Soc. 2013, 135, 10664−10672

microboxes using $NaAlO_2$ and $NaBO_2{\cdot}4H_2O$ as the alkaline precursors (Figure S21 in Supporting Information). The synthesis is usually very facile and rapid, and the reaction can be generally completed within 10 min at room temperature. Furthermore, the present synthesis can be simply scaled up to achieve the high-yield, gram-scale production of these multicompositional microboxes. The versatility of this approach toward multicompositional microboxes provides the possibility to design and tailor the compositions and the derived functionalities for desirable applications.

The complexity of the hollow microboxes in both structure and composition might endow the materials with exceptional properties and performance in particular applications. Both SnO_2 and Fe_2O_3 are important functional materials that have been studied in many areas, for example, as promising anode materials for lithium ion batteries.[26−28] In this work, we further demonstrate the remarkable lithium storage properties of these hollow microboxes, which are associated with their unique nanostructure and high complexity. SnO_2 can reversibly store lithium mainly via the alloying process after the initial electrochemical reduction to metallic Sn nanoparticles, while iron oxide can reversibly react with lithium through the conversion reaction.[28] Despite the distinct electrochemical processes involved, they can generally deliver very high specific capacity (800−1000 mA h g^{-1}) far exceeding that of the conventional graphite anode (theoretically 372 mA h g^{-1}). However, the exceptional lithium storage property is accompanied by some severe drawbacks, including the huge volume variation upon lithium insertion/extraction that leads to the crack and disintegration of the electrode film and the low electrochemical activity of large grains.[29] Previous studies suggest that the electrochemical performance can be improved via formation of hollow structures and/or nanocomposites.[19,30,31] The pure Fe_2O_3 microboxes obtained from route A exhibit the representative electrochemical behavior of iron oxide, with reasonable cycling performance (Figure 6). As shown in Figure 6A, from the discharge−charge voltage profiles of single-shelled Fe_2O_3 microboxes, a distinct voltage plateau can be clearly identified at about 0.75 V during the initial discharge process, which shifts to about 1.0 V and remains stable in the subsequent cycles. Meanwhile, a poorly defined plateau is observed in the charge process at about 1.8 V. The discharge−charge voltage profiles are in good agreement with those in previous reports, which correspond to the reversible reduction of Fe_2O_3 to Fe^0 and the simultaneous formation of Li_2O based on the conversion reaction described as follows: $Fe_2O_3 + 6Li^+ + 6e^- \leftrightarrow 2Fe^0 + 3Li_2O$. Figure 6B shows that multiple-shelled Fe_2O_3 microboxes exhibit significantly improved cycling performance compared to single-shelled and double-shelled Fe_2O_3 microboxes. The initial discharge and charge capacities of multiple-shelled Fe_2O_3 microboxes are found to be 1473 and 917 mA h g^{-1}, respectively. The irreversible capacity loss of 35% is mainly attributed to irreversible processes such as the decomposition of electrolyte and the inevitable formation of solid-electrolyte interface (SEI) film, which are common to most anode materials. From the second cycle onward, the Fe_2O_3 microboxes exhibit a high Coulombic efficiency of ∼95%. At the end of the 30th charge−discharge cycle, a reversible capacity of 650 mA h g^{-1} can still be retained for the multiple-shelled Fe_2O_3 microboxes, while comparable capacities of 355 and 519 mA h g^{-1} are obtained for single-shelled and double-shelled Fe_2O_3 microboxes, respectively. One could probably attribute this reasonably

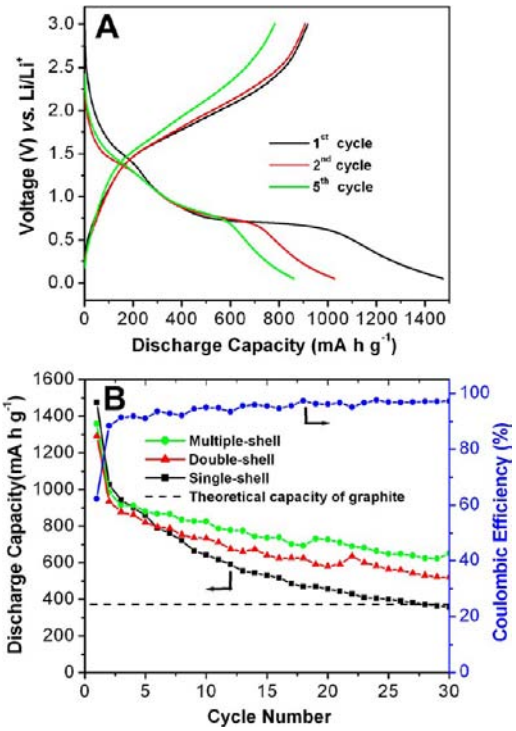

Figure 6. (A) Discharge/charge voltage profiles of single-shelled Fe_2O_3 microboxes (0.2 M NaOH). (B) Cycling performance of single-shelled (0.2 M NaOH), double-shelled, and multiple-shelled Fe_2O_3 microboxes synthesized under hydrothermal conditions and Coulombic efficiency of single-shelled Fe_2O_3 microboxes in the voltage window of 0.05−3.0 V vs Li/Li^+ at the same current density of 200 mA g^{-1}.

good performance of Fe_2O_3 microboxes to the thin nanosheet subunits that facilitate the electrolyte penetration and Li^+ ions transport in the electrode and the hierarchical hollow structures that could efficiently buffer the stress caused by the volume variation during the charge−discharge process. Notably, microboxes with multiple shells show better capacity retention due to the maximization of the beneficial effects arising from the hollow and hierarchical structures, which could better withstand the repeated volume expansion/contraction and facilitate the lithium ions insertion with reduced diffusion length.

Incorporating SnO_2 into the microboxes via route B further improves the electrochemical performance. Compared with that of Fe_2O_3 microboxes (Figure 6), the prolonged sloping region at low voltage (below ∼0.6 V) in the discharge curves of Fe_2O_3/SnO_2 microboxes (Figure 7) is mainly contributed by the Sn-based component. The differential capacity versus voltage curves of first, second, and fifth cycles (Figure S22 in Supporting Information) further confirm the electrochemical processes involving both Fe_2O_3 and SnO_2. The initial discharge and charge capacities of Fe_2O_3/SnO_2 microboxes are found to be 1751 and 904 mA h g^{-1}, respectively (Figure 7A). Besides the above-mentioned irreversible processes, the initial reduction of SnO_2 to metallic Sn also accounts for the higher irreversible loss of 45%. From the second cycle onward, the Fe_2O_3/SnO_2 microboxes exhibit a high Coulombic efficiency of ∼95%. Remarkably, the Fe_2O_3/SnO_2 microboxes deliver much superior cycling stability compared to single-compositional Fe_2O_3 and SnO_2 microboxes, with a reversible capacity of 500 mA h g^{-1} at the end of the 100th cycle (Figure 7B). This

dx.doi.org/10.1021/ja401727n | J. Am. Chem. Soc. 2013, 135, 10664−10672

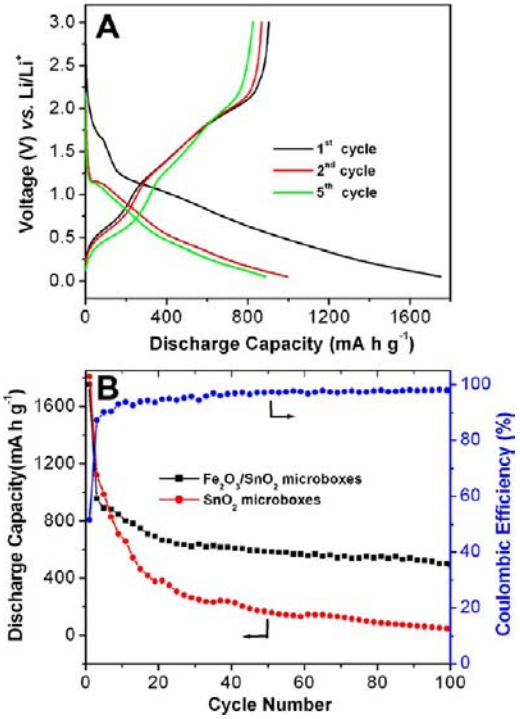

Figure 7. (A) Discharge/charge voltage profiles of Fe_2O_3/SnO_2 microboxes. (B) Cycling performance of Fe_2O_3/SnO_2 microboxes and SnO_2 microboxes and Coulombic efficiency of Fe_2O_3/SnO_2 microboxes in the voltage window of 0.05−3.0 V vs Li/Li^+ at the same current density of 200 mA g^{-1}.

capacity retention is impressive for both iron and tin oxide based materials, especially taking into account the absence of additional carbon modifications (e.g., carbon coating, formation of composites with carbon nanotubes or graphene).[26−31] Besides the advantages of hollow structure as discussed earlier, the possible synergic effects that arise from the highly integrated Fe_2O_3 and SnO_2 may also account for the exceptional lithium storage capability of the multicompositional microboxes, although the detailed mechanism is still under investigation.[30]

CONCLUSIONS

We demonstrate a general approach toward the large-scale and facile synthesis of complex hollow microboxes via manipulating the template-engaged reactions between the PB template and different alkaline substances. The reaction between PB microcubes with NaOH solution leads to the formation of $Fe(OH)_3$ microboxes with controllable multishelled structure. Meanwhile, PB microcubes react with the conjugate bases of metal oxide based weak acids and generate multicompositional microboxes (Fe_2O_3/SnO_2, Fe_2O_3/SiO_2, Fe_2O_3/GeO_2, Fe_2O_3/Al_2O_3, and Fe_2O_3/B_2O_3), which consist of uniformly dispersed oxides/hydroxides of iron and another designed element. Such complex hollow structures and atomically integrated multiple compositions might bring usual physiochemical properties. As an example, we demonstrate that these complex hollow microboxes, especially the Fe_2O_3/SnO_2 composite microboxes, exhibit remarkable electrochemical performance as anode materials for lithium ion batteries. We further anticipate that these hollow microboxes with high structural and compositional complexity would find their promising applications in many areas.

ASSOCIATED CONTENT

Supporting Information

Additional FESEM images, TEM images, XRD patterns, N_2 adsorption−desorption isotherms, EDX spectra, optical photographs, and differential capacity versus voltage plots curves. This material is available free of charge via the Internet at http://pubs.acs.org.

AUTHOR INFORMATION

Corresponding Author

xwlou@ntu.edu.sg

Author Contributions

†L.Z. and H.B.W. contributed equally to this work.

Notes

The authors declare no competing financial interest.

ACKNOWLEDGMENTS

We are grateful to the National Research Foundation (Singapore) for financial support through the Clean Energy Research Programme (CERP, Grant NRF2009EWRCERP001-036).

REFERENCES

(1) Caruso, F.; Caruso, R. A.; Mohwald, H. *Science* **1998**, *282*, 1111.
(2) Sun, Y. G.; Xia, Y. N. *Science* **2002**, *298*, 2176.
(3) Son, D. H.; Hughes, S. M.; Yin, Y. D.; Alivisatos, A. P. *Science* **2004**, *306*, 1009.
(4) Yin, Y. D.; Rioux, R. M.; Erdonmez, C. K.; Hughes, S.; Somorjai, G. A.; Alivisatos, A. P. *Science* **2004**, *304*, 711.
(5) Gonzalez, E.; Arbiol, J.; Puntes, V. F. *Science* **2011**, *334*, 1377.
(6) Walsh, D.; Mann, S. *Nature* **1995**, *377*, 320.
(7) Yang, J.; Ying, J. Y. *Nat. Mater.* **2009**, *8*, 683.
(8) Marinakos, S. M.; Novak, J. P.; Brousseau, L. C.; House, A. B.; Edeki, E. M.; Feldhaus, J. C.; Feldheim, D. L. *J. Am. Chem. Soc.* **1999**, *121*, 8518.
(9) Ameloot, R.; Vermoortele, F.; Vanhove, W.; Roeffaers, M. B. J.; Sels, B. F.; De Vos, D. E. *Nat. Chem.* **2011**, *3*, 382.
(10) Xu, H. L.; Wang, W. Z. *Angew. Chem., Int. Ed.* **2007**, *46*, 1489.
(11) Skrabalak, S. E.; Au, L.; Li, X. D.; Xia, Y. N. *Nat. Protoc.* **2007**, *2*, 2182.
(12) An, K.; Kwon, S. G.; Park, M.; Bin Na, H.; Baik, S. I.; Yu, J. H.; Kim, D.; Son, J. S.; Kim, Y. W.; Song, I. C.; Moon, W. K.; Park, H. M.; Hyeon, T. *Nano Lett.* **2008**, *8*, 4252.
(13) Hu, M.; Belik, A. A.; Imura, M.; Yamauchi, Y. *J. Am. Chem. Soc.* **2013**, *135*, 384.
(14) Xiong, S. L.; Zeng, H. C. *Angew. Chem., Int. Ed.* **2012**, *51*, 949.
(15) Park, J.; Zheng, H.; Jun, Y. W.; Alivisatos, A. P. *J. Am. Chem. Soc.* **2009**, *131*, 13943.
(16) Yang, H. G.; Zeng, H. C. *Angew. Chem., Int. Ed.* **2004**, *43*, 5930.
(17) Wang, L. Z.; Tang, F. Q.; Ozawa, K.; Chen, Z. G.; Mukherj, A.; Zhu, Y. C.; Zou, J.; Cheng, H. M.; Lu, G. Q. *Angew. Chem., Int. Ed.* **2009**, *48*, 7048.
(18) Cho, W.; Lee, Y. H.; Lee, H. J.; Oh, M. *Adv. Mater.* **2011**, *23*, 1720.
(19) Lou, X. W.; Archer, L. A.; Yang, Z. C. *Adv. Mater.* **2008**, *20*, 3987.
(20) Zhao, Y.; Jiang, L. *Adv. Mater.* **2009**, *21*, 3621.
(21) Sun, Y. G.; Wiley, B.; Li, Z. Y.; Xia, Y. N. *J. Am. Chem. Soc.* **2004**, *126*, 9399.
(22) Zhang, N.; Ouyang, S. X.; Li, P.; Zhang, Y. J.; Xi, G. C.; Kako, T.; Ye, J. H. *Chem. Commun.* **2011**, *47*, 2041.
(23) Zhang, L.; Wu, H. B.; Madhavi, S.; Hng, H. H.; Lou, X. W. *J. Am. Chem. Soc.* **2012**, *134*, 17388.
(24) Buser, H. J.; Schwarzenbach, D.; Petter, W.; Ludi, A. *Inorg. Chem.* **1977**, *16*, 2704.

(25) Matsumura, T.; Sonoyama, N.; Kanno, R.; Takano, M. *Solid State Ionics* **2003**, *158*, 253.
(26) Idota, Y.; Kubota, T.; Matsufuji, A.; Maekawa, Y.; Miyasaka, T. *Science* **1997**, *276*, 1395.
(27) Poizot, P.; Laruelle, S.; Grugeon, S.; Dupont, L.; Tarascon, J. M. *Nature* **2000**, *407*, 496.
(28) Armand, M.; Tarascon, J. M. *Nature* **2008**, *451*, 652.
(29) Larcher, D.; Beattie, S.; Morcrette, M.; Edstroem, K.; Jumas, J. C.; Tarascon, J. M. *J. Mater. Chem.* **2007**, *17*, 3759.
(30) (a) Zhou, W.; Cheng, C.; Liu, J. P.; Tay, Y. Y.; Jiang, J.; Jia, X. T.; Zhang, J. X.; Gong, H.; Hng, H. H.; Yu, T.; Fan, H. J. *Adv. Funct. Mater.* **2011**, *21*, 2439. (b) Chen, J. S.; Li, C. M.; Zhou, W. W.; Yan, Q. Y.; Archer, L. A.; Lou, X. W. *Nanoscale* **2009**, *1*, 280.
(31) Ding, S. J.; Chen, J. S.; Qi, G. G.; Duan, X. N.; Wang, Z. Y.; Giannelis, E. P.; Archer, L. A.; Lou, X. W. *J. Am. Chem. Soc.* **2011**, *133*, 21.